Identification of Vanadium Oxide Species and Trapped Single Electrons in Interaction with the $CeVO_4$ Phase in Vanadium−Cerium Oxide Systems. ^{51}V MAS NMR, EPR, Raman, and Thermal Analysis Studies

J. Matta, D. Courcot,* E. Abi-Aad, and A. Aboukaïs

Laboratoire de Catalyse et Environnement - E.A.2598, Université du Littoral - Côte d'Opale, MREID, 145, avenue Maurice Schumann, F-59140 Dunkerque, France

Received November 26, 2001. Revised Manuscript Received July 10, 2002

Vanadium−cerium oxide catalysts, with different V/Ce atomic ratios, were prepared using vanadyl oxalate (VOC_2O_4) impregnated on ceria (CeO_2) as precursors. Subsequently, the freshly prepared solids were calcined under a flow of dried air at different temperatures from 400 to 800 °C. These solids have been characterized with different techniques: Raman spectroscopy, thermal analysis (TG-DSC), specific area measurements (BET), EPR, and solid-state ^{51}V MAS NMR. Different vanadium species in the vanadium−cerium oxide catalysts have been evidenced. Polymeric V−O−V chains, vanadium tetrahedral surface species, and V_2O_5 phase are stabilized mainly when solids are calcined in the temperature range 400−500 °C. Their formation also depends on the vanadium content. For higher calcinations temperatures (≥500°C), CeO_2 reacts with vanadium (V) species to form a $CeVO_4$ mixed phase. Further to that formation, a single electron is trapped in an oxygen vacancy in the $CeVO_4$ phase and can be considered as its probe.

Introduction

The oxides such as CeO_2 and V_2O_5 are commonly used as catalysts in depollution reactions. These systems can lead to interesting catalytic properties in the oxidation of diesel soot particles. In fact, the presence of ceria (CeO_2) has been found effective either in the promotion of various catalytic reactions or as an additive in the so-called three-way catalysts (TWC) for automotive exhaust treatment.[1−3] It is a known feature that ceria exhibits a large deviation from its CeO_2 stoichiometric composition by the creation of oxygen vacancies and particularly the relatively high mobility of bulk oxygen species.[4,5] This behavior results in making CeO_2 a promising material for use either as a support or active catalyst in oxidation−reduction reactions,[6,7] thus broadening the region around the air/fuel stoichiometric value in which the catalysts are effective.

In parallel, vanadia supported on various oxide carriers is widely used as a catalyst in different oxidation processes.[8,9] It has also proved to be quite effective for the selective catalytic reduction (SCR) of nitric oxide NO.[10] It has been demonstrated that the selectivity and activity of these catalysts depend on, among other factors, the vanadium loading, calcination temperature, type of support, and its surface acidity.[11] In addition, depending on the nature of the oxide carrier (i.e., Al_2O_3, TiO_2, MgO, ZrO_2), vanadia catalysts may exhibit different catalytic properties, since the metal oxide−support interaction affects both dispersion and redox behavior of the active phase and also work function properties.[12]

However, surface vanadium oxide stability can be limited if ternary compounds of the type $M_xV_yO_z$ are formed between the carrier and the vanadia phase. Indeed, in a previous work,[13] we observed that V_2O_5 can react with CeO_2 carrier at high temperature (≥ 600 °C) to form the vanadium orthovanadate $CeVO_4$ compound. Thus, it provided deep modifications of the supported vanadia phase. For these reasons, investigation on the nature of surface vanadium species and their stability in V−Ce−O systems causes great interest. Such studies could be provided by the determination of the local structure of these species following the calcination treatment and the vanadium content. The major structural information about these surface metal oxide species has been derived from Raman spectroscopy studies, because the molecular nature of species can be

* Corresponding author. E-mail: courcot@univ-littoral.fr.

(1) Shelef, M.; Graham, G. W. *Catal. Rev. Sci. Eng.* **1994**, *36*, 433.
(2) Trovalleri, A. *Catal. Rev. Sci. Eng.* **1996**, *38*, 439.
(3) Kaspar, J.; Fornasiero, P.; Graziani, M. *Catal. Today* **1999**, *50*(2), 285.
(4) Harrison, P. G.; Creaser, D. A.; Wolfindale, B. A.; Waugh, K. C.; Morris, M. A.; Mackrodt, W. C. *Catalysis Surface Characterization*; Dines, T. J., et al., Eds.; Royal Society of Chemistry: Cambridge, 1992; p 76.
(5) Körner, R.; Ricken, N.; Nölting, J.; Riess, I. *J. Solid State Chem.* **1989**, *78*, 136.
(6) Yao, H. C.; Yu Yao, Y. F. *J. Catal.* **1984,** *86*, 254.
(7) González-Velasco, J. R.; Gutiérrez-Ortiz, M. A.; Marc, J. L.; Botas, J. A.; Gonzalez-Marcos, M. P.; Blanchard, G. *Appl. Catal. B* **1999**, *22*, 167.
(8) Grzybowska- Swierkosz, B. *Appl. Catal., A Gen.* **1997**, *157*, 263.
(9) Ahlström, A. F.; Odenbrand, O. *Appl. Catal.* **1990**, *60*, 157.
(10) Lietti, L.; Forzatti, P. *J. Catal.* **1994**, *147*, 241.
(11) van Hengstum, A. J.; van Ommen, J.; Bosch, G. H.; Gellings, P. J. *Appl. Catal.* **1983**, *8*, 369.
(12) Arena, F.; Giordano, N.; Parmaliana, A. *J. Catal.* **1997**, *166*, 66.
(13) Cousin, R.; Dourdin, M.; Abi-Aad, E.; Courcot, D.; Capelle, S.; Guelton, M.; Aboukaïs, A. *J. Chem. Soc., Faraday Trans.* **1997**, *93*, 3863.

10.1021/cm010396t CCC: $22.00
Published on Web 09/26/2002

Table 1. Chemical Composition of the Studied Samples

samples	chemical composition	samples	chemical composition
1V10Ce	1.08V10Ce	3V10Ce	2.73V10Ce
2V10Ce	1.67V10Ce	5V10Ce	5.06V10Ce

determined by this characterization method.[14] Solid-state ^{51}V NMR has also been used by various investigators,[15−17] toward the determination of the molecular structure of these surface metal oxide species on oxide support due to the favorable magnetic properties of the ^{51}V nucleus. In addition, magic angle spinning experiments (MAS NMR) provided precise discrimination between different species that may simultaneously be present in the sample.[17] In fundamental studies in heterogeneous catalysis, it is desirable to establish relationships between surface structures and the catalytic properties of a system. In this spirit, the determination of the nature of vanadia species can provide also useful information leading to a better understanding of the elementary steps of heterogeneously catalyzed reactions.

In this work, physicochemical properties of ceria-supported vanadia systems, associating the oxidation states Ce^{4+}/Ce^{3+} and V^{5+}/V^{4+}, are studied. The aim is to highlight the nature of the surface vanadium species and evaluate their stability depending on either the vanadium content or the calcination temperature used for the treatment of solids. Different characterization techniques were then used, such as Raman, TG-DSC, BET surface area measurements, and resonance methods, such as EPR and ^{51}V MAS NMR.

Experimental Section

Ceria (CeO_2) was prepared by precipitation of cerium hydroxide from $Ce(NO_3)_3{\cdot}6H_2O$ with a NaOH solution as described in ref 18. The solid was calcined at 500 °C for 4 h under a flow of dried air. Subsequently, vanadyl oxalate VOC_2O_4 was impregnated on ceria to prepare *x*V10Ce samples with different V/Ce atomic ratios (nearly $x = 1$, 2, 3, and 5). After drying at 100 °C, the solids freshly prepared were calcined between 400 and 800 °C under a flow of dried air for 4 h. Table 1 indicates the precise vanadium content in the samples, calcined at 500 °C, obtained by chemical analysis.

The Raman spectra were recorded using a Dilor XY monochromator with subtractive dispersion. The samples are excited using the 632.8 nm radiation of a He−Ne laser. X-ray powder diffraction analysis was carried out on a D5000 Siemens diffractometer equipped with a copper anticathode and a secondary beam monochromator.

Thermal analysis measurements were performed using a Netzsch STA 409 apparatus equipped with a microbalance. Simultaneous thermogravimetric and differential scanning calorimetric (TG-DSC) curves were obtained while the dried *x*V10Ce samples were heated from room temperature to 800 °C with a rate of 5 °C min^{-1} under a flow of air (75 mL min^{-1}).

The specific areas of solids were determined by the BET method using an Ankersmit Quantasorb jr apparatus, and the gas adsorbed at −196 °C was pure nitrogen (N60).

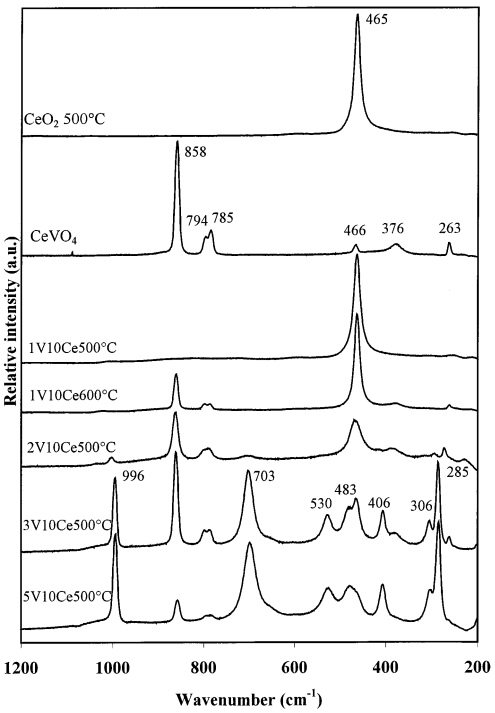

Figure 1. Raman spectra of CeO_2 calcined at 500 °C, $CeVO_4$ phase, and the *x*V10Ce samples calcined at different temperatures.

The electron paramagnetic resonance (EPR) measurements were performed at −269, −196, and 20 °C on a EMX Bruker spectrometer, using a cavity operating with a frequency of ∼9.5 GHz (X-band). The magnetic field was modulated at 100 kHz. The *g* values are determined from precise frequency and magnetic field values.

Magic angle spinning (MAS) ^{51}V NMR spectra were recorded at room temperature on a Bruker ASX-400 spectrometer operating at 105.2 MHz and equipped with a MAS probe for 4 mm outer diameter rotors. Rotation frequencies up to 17 kHz have been used. In all experiments, a single pulsed excitation of 1.5 μs was applied, and a dead time of 10 μs and a recycle time of 5s were used. The isotropic chemical shifts were referred to external $VOCl_3$.

Results and Discussion

1. Raman Spectroscopy. Figure 1 shows the Raman spectral features found in the range 200−1200 cm^{-1} for the different *x*V10Ce samples. A ceria phase has been evidenced in all the solids. In fact, the Raman spectrum of CeO_2 is characterized by the 465 cm^{-1} band, which corresponds to F_{2g} symmetry in the cubic phase.[19] For the 1V10Ce solid, only the ceria CeO_2 phase was evidenced after calcination at 500 °C, whereas for higher vanadium contents ($x = 2$, 3, and 5), numerous Raman bands (996, 703, 530, 483, 406, 306, and 285 cm^{-1}) appeared beside the characteristic band attributed to ceria and could be unambiguously attributed to polycrystalline V_2O_5.[20] Nevertheless, for higher vanadium content, Raman spectra indicated the presence of other bands at 858, 794, 785, 466, 376, and 263 cm^{-1}. Taking into consideration the possibility of the formation of the $CeVO_4$ by reaction between V_2O_5 and CeO_2, a $CeVO_4$

(14) Dixit, L.; Gerrard, D.; Bowley, H. *Appl. Spectrosc. Rev*. **1986**, *22*, 189.
(15) Eckert, H.; Wachs, I. *J. Phys. Chem*. **1989**, *93*, 6786.
(16) Mastikhin, V.; Terskikh, V.; Lapina, O. B.; Filiminova, S.; Seidl, M.; Knozinger, H. *J. Catal.* **1995**, *156*, 1.
(17) Courcot, D.; Grzybowska, B.; Barbaux, Y.; Rigole, M.; Ponchel, A.; Guelton, M. *J. Chem. Soc., Faraday Trans*. **1996**, *92*(6), 1609.
(18) Abi-Aad, E.; Bechara, R.; Grimblot, J.; Aboukaïs, A. *Chem. Mater*. **1993**, *5*, 793.
(19) Fornasiero, P.; Balducci, G.; Di Monte, R.; Kaspar, J.; Sergo, V.; Gubitosa, G.; Ferrero, A.; Graziani, M. *J. Catal.* **1995**, *164*, 173.
(20) Roozeboom, F.; Mitteimeijer, M. C.; Moulijn, J.; Medema, A. J.; De Beer, V. H. J.; Gellings, P. J. *J. Phys. Chem*. **1980**, *84*, 2783.

Table 2. Thermogravimetric Data of the Solids *x*V10Ce[a]

		weight loss (%)				weight loss (%)	
samples	temp (°C)	exptl	calcd	samples	temp (°C)	expl	calcd
1V10Ce	50−170	1.22		3V10Ce	50−170	2.99	
	170−340	3.98	3.61		170−350	10.39	7.91
	600−800	0.46	0.45		500−800	0.94	0.96
2V10Ce	50−170	1.90		5V10Ce	50−170	4.05	
	170−350	5.36	5.30		170−310	14.52	12.41
	500−800	0.71	0.66		500−800	1.27	1.50

[a] Theoretical losses were calculated using the chemical composition data from Table 1. For each sample, three temperature ranges were considered (see text): from 50 to 170 °C (water removal); from 170 to 310−350 °C (VOC_2O_4 decomposition); and from 500−600 to 800 °C (formation of $CeVO_4$).

sample used as reference has been studied (Figure 1). The spectroscopic "fingerprint" obtained clearly corresponds to the bands observed in 2V10Ce, 3V10Ce, and 5V10Ce, which reveals the presence of $CeVO_4$ in these samples. It can be mentioned that the bands at 858, 794, and 785 cm^{-1} are generally assigned to the elongation mode of vanadium oxide species with tetrahedral coordination,[21] which is in agreement with the structure of $CeVO_4$.[22]

From a comparison of the intensities of Raman bands relative to V_2O_5 and $CeVO_4$ phases obtained for *x*V10Ce samples treated at 500 °C, it seems that a major part of vanadium in 2V10Ce is present as $CeVO_4$. Upon increasing the vanadium content, vanadium seems to be more agglomerated as V_2O_5 crystalline particles. On the other hand, for the lower vanadium content, measurements on 1V10Ce showed some difference, since no vanadium phase could be detected after calcination at 500 °C. However, it was found that $CeVO_4$ was formed from a thermal treatment at 600 °C. Although the vanadium species formed at 500 °C was not observed by Raman, it may be suggested that it corresponds to dispersed vanadium species that exhibit a better stability than those formed on other *x*V10Ce samples.

2. TG-DSC. Figure 2 and Table 2 illustrate the TG-DSC results obtained for freshly prepared *x*V10Ce samples. For all the samples, a first weight loss obtained from room temperature until 170°C, simultaneously associated with a broad endothermic peak, can be attributed to the removal of water. A second weight loss starts from 170°C and is achieved between 310 and 350 °C, depending on the samples. In parallel, the three exothermic peaks observed in the range of 170−350 °C on all these samples have already been evidenced elsewhere[23] and attributed to the decomposition of vanadium(V) oxalate (187 °C), vanadyl oxalate (270−290 °C), and cerium oxalate (310 °C). A vanadium(V) oxalate type arises from a partial oxidation phenomenon occurring when vanadyl oxalate is deposited on ceria (CeO_2). Moreover, the observation of cerium oxalate decomposition at 310 °C[23,24] can be explained by the reaction of oxalate ions with CeO_2 surface during the preparation of V−Ce samples. The global loss between 170 and 310−350 °C appears closely related to the vanadium content as it increases with the higher vanadium loading in solids and corresponds to the

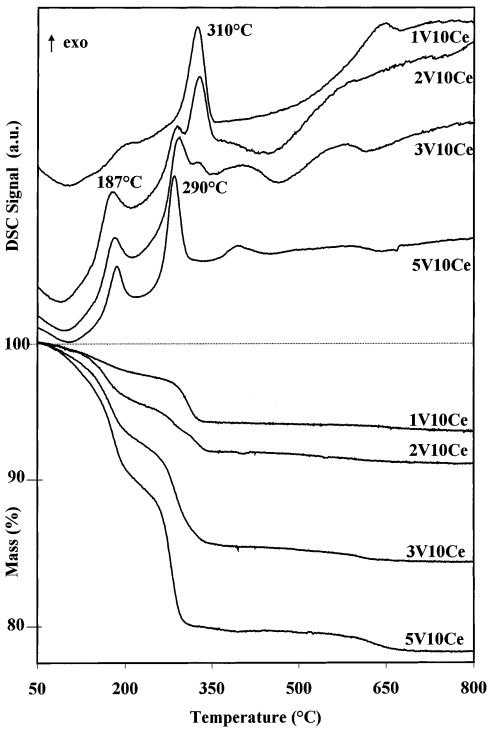

Figure 2. Thermal decomposition under air: TG-DSC of the dried *x*V10Ce samples. Heating rate: 5 °C min^{-1}.

formation of vanadium oxide following the reaction:

$$2VOC_2O_4/CeO_2 \rightarrow V_2O_5/CeO_2 + 2CO_2 + {}^1/_2O_2$$

The presence of vanadium oxide as V_2O_5 crystalline particles was confirmed by Raman technique on all the samples, except for 1V10Ce. Nevertheless, the weight loss obtained for this latter sample after the decomposition of the VOC_2O_4 compound corresponds exactly to that theoretically calculated from the above reaction. Despite the absence of crystallized phase in 1V10Ce, this result tends to show that vanadium(V) oxide species are formed in the sample. The identification of this species will be investigated and provided from ^{51}V NMR experiments in section 5.

At a higher temperature range (500−800 °C), a weak weight loss occurs and seems to be depending on the vanadium content. The loss is 0.46 wt % for 1V10Ce and 1.27 wt % for 5V10Ce (Table 2). At this step of the thermal treatment, a possible interpretation of this phenomenon is the departure of oxygen from the solid. In fact, in a previous work,[13] it was demonstrated that CeO_2 and V_2O_5 could react together in the solid state in the temperature range 500−800 °C to form cerium

(21) Baran, E. J.; Escobar, M. E.; Fourier, L. L.; Filgueira, R. R. *Z. Anorg. Allg. Chemie* **1981**, *472*, 193.
(22) Toubol, A. *Rev. Chim. Minér.* **1985**, *22*, 610.
(23) Matta, J.; Courcot, D.; Abi-Aad, E.; Aboukaïs, A. *J. Therm. Anal. Calorim.* **2001**, *66*, 717.
(24) Overs, A.; Riess, I. *J. Am. Ceram. Soc.* **1982**, *65*, 606.

orthovanadate ($CeVO_4$). Hence, this reaction occurred till the complete consumption of the default reactant and could be expressed by the following equation:

$$V_2O_5 + 2CeO_2 \rightarrow 2CeVO_4 + {}^1/_2O_2$$

From the elementary chemical composition (Table 1), we can assume that all the V_2O_5 reacts during the TG-DSC measurements. An additional argument is also given by DSC curves of 1V10Ce, 2V10Ce, and 3V10Ce, because of the absence of the endotherm related to the melting of V_2O_5, which typically occurs at 670 °C.[25] However, a small endothermic peak is observed at 669 °C in 5V10Ce, since the formation reaction of $CeVO_4$ goes on longer, as revealed by the TG curve (Figure 2). It is then possible to calculate the weight loss percentage corresponding to the departure of oxygen as gaseous O_2 (Table 2). Within the experimental errors, a good agreement between the experimental and theoretical values is obtained mainly in the case of 1V10Ce, 2V10Ce, and 3V10Ce samples. If the difference observed in the case of 5V10Ce sample is considered to be a significant information, it could be suggested that, during the treatment of the sample at 5 °C min^{-1} in air, the sample is submitted to a fast increase of temperature, whereas a great modification of the solid occurred [(VO^{2+} + $C_2O_4{}^{2-}$) → vanadium(V) oxide → $CeVO_4$]. A lower experimental weight loss value than the theoretical one can be attributed to the presence of a substoichiometric vanadium oxide (V_2O_{5-x}) formed under these experimental conditions. In addition, it could be noted that the loss related to the formation of $CeVO_4$ started from 575 °C and goes on progressively in the case of 5V10Ce, whereas in 1V10Ce solid, the loss occurred only from 625 °C and is abrupt.

To sum up, the study of freshly prepared *x*V10Ce solids by simultaneous TG-DSC techniques shows the complete decomposition of VOC_2O_4 precursor when a temperature of 350 °C is reached. The stability of the sample weight is obtained between 350 and 500 °C. Finally, the slight weight loss in the range of 500−700 °C is in agreement with the transformation of V_2O_5 and CeO_2 to give $CeVO_4$ mixed oxide.

3. Specific Area. Figure 3 shows the variation of specific areas of *x*V10Ce samples versus the calcination temperature. The CeO_2 solid used for the preparation of the vanadia−ceria catalysts exhibits a specific area of 100 m^2/g after the calcination treatment at 500 °C. For *x*V10Ce samples dried at 100 °C, the specific areas decrease upon increasing the vanadium content (i.e. 1V10Ce, 70 m^2/g; 5V10Ce, 20 m^2/g). However, for all the samples, the specific area values are much higher once samples have been calcined at 400 or 500 °C. This increase in specific area in comparison with uncalcined samples can be explained by the departure of physisorbed water and to the decomposition of the vanadyl oxalate precursor. This attribution is supported by the results of the thermal analysis data showing the occurrence of these two phenomena for temperature treatments <400 °C. For high-temperature treatments (≥600°C), a decrease of the specific area is observed, particularly for the samples with high vanadium content

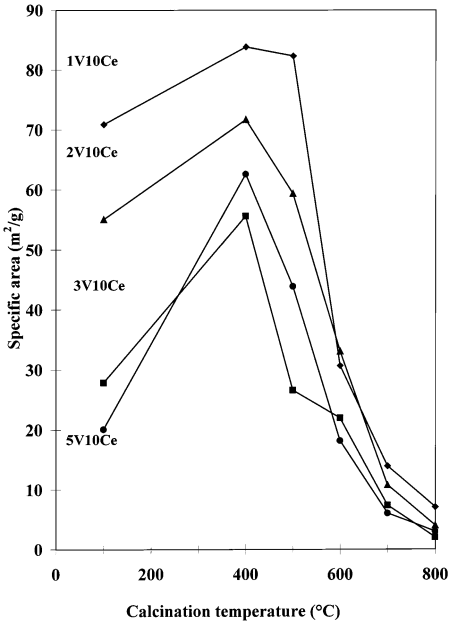

Figure 3. Evolution of the specific area of the *x*V10Ce samples with the calcination temperature.

(Figure 3). In fact, specific areas less than 10 m^2/g are obtained for catalysts calcined at 800 °C. As the formation of a $CeVO_4$ phase has been mentioned above, a $CeVO_4$ sample prepared and characterized in our laboratory has been considered as reference compound. The measure of its specific area indicated a value of 5 m^2/g. Thus, the decrease of the specific area of the solids *x*V10Ce with the increase of calcination temperature above 500 °C can be related to the formation of the $CeVO_4$ phase and the growth of CeO_2 grains, since ceria possesses a specific area of 14 m^2/g after calcinations at 800 °C. Besides, the formation of $CeVO_4$ at relatively low temperature could be probably favored by the preparation method, since the vanadium oxide precursor was impregnated on CeO_2 nanoparticles. Nevertheless, it is interesting to note that the specific area of 1V10Ce remains nearly the same after calcination treatment at 400 and 500 °C, while the decrease in surface area only occurred after treatment at 600 °C. This behavior can be explained by considering the Raman data (Figure 1). On the contrary to other *x*V10Ce samples, the appearance of the $CeVO_4$ phase was obtained only from 600 °C in 1V10Ce. Thus, the relatively high specific area of 1V10Ce after treatment at 500 °C could be essentially explained by the absence of $CeVO_4$ in the sample.

4. EPR. The EPR parameter values have been precisely determined from the calculated spectra, which were simulated with the Bruker SIMFONIA program based upon perturbation theory.[26] In fact, the theoretical EPR signals can be calculated using the effective spin Hamiltonian $H = \beta H_j S_j g_j$ where *j* is the component along one of the three axis *x*, *y*, and *z*, H is the applied magnetic field, *S* is the total spin electron, *g* is the spectroscopic factor, and β is the Bohr magneton. A polyoriented sample EPR signal has been simulated by generating 9000 random orientations of the magnetic field and by summing the corresponding 9000 absorp-

(25) *Hanbook of Chemistry and Physics*, 77th ed.; Lide, D. R., Ed.; CRC Press: Boca Raton, 1996−1997.

(26) Weber, R. T. *WIN-EPR SIMFONIA manual*, Ver.1.2; Bruker Instruments, INC.: Billerica, MA, 1995, and references therein.

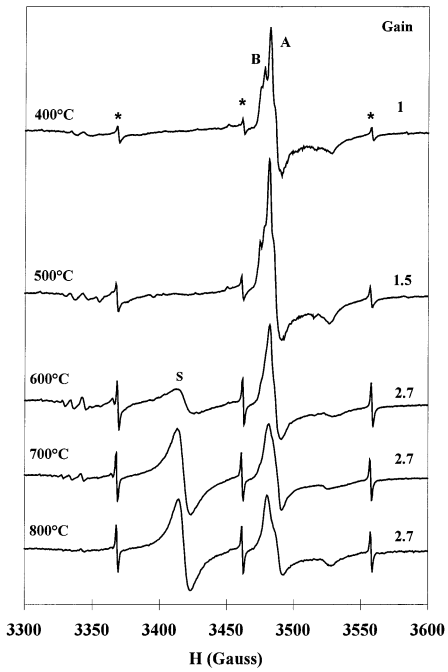

Figure 4. EPR spectra recorded at −196 °C for 1V10Ce sample calcined at different temperatures.

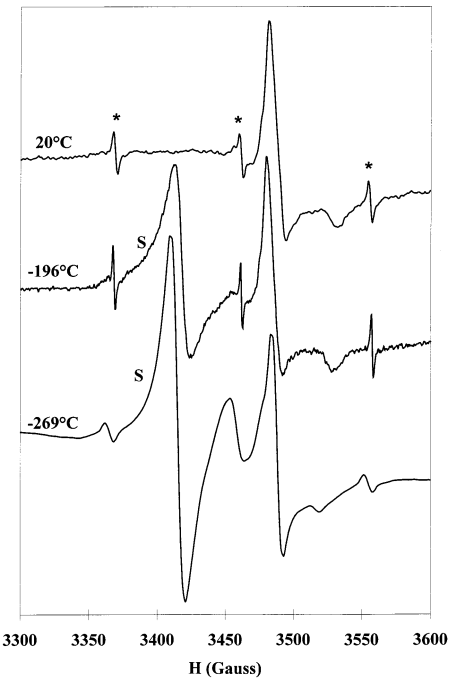

Figure 5. EPR spectrum of 3V10Ce sample calcined at 700 °C, recorded at −269, −196, and 20 °C.

tion signals. The final signal was obtained by performing a convolution (Gaussian or Lorentzian line shape) of each transition line, adding all contributions, and calculating the first derivative of the signal; the line width of each component has been optimized in order to obtain the best accordance with the observed experimental values.

Figure 4 shows the EPR spectra recorded at −196 °C for 1V10Ce sample calcined at different temperatures. For a calcination temperature of 400 °C, two superimposed signals with $g < 2$ denoted by A and B are observed on the solids. In addition, a minor impurity of Mn^{2+} ions (denoted by * and amounting to ca. 0.8 ppm) is also detected, since the EPR technique is highly sensitive and capable of detecting the paramagnetic centers even at very low concentration.

The A and B signals are apparently characterized as $g_{\perp(A)} = 1.967$ and $g_{\parallel(A)} = 1.940$ and $g_{\perp(B)} = 1.972$ and $g_{\parallel(B)}$=1.947, respectively. The effective g values, deduced from the calculated spectra, are $g_{xx(A)} = 1.9654$, $g_{yy(A)} = 1.9626$, $g_{zz(A)} = 1.9398$ and $g_{xx(B)} = 1.9692$, $g_{yy(B)} = 1.9670$, $g_{zz(B)} = 1.9465$. These signals can be attributed to the presence of two different Ce^{3+} [f^1 ions; $g_e > g_\perp > g_\parallel$] sites in the solid. Similar signals were observed in the literature[27,28] and assigned to Ce^{3+} ions or, more precisely, to an interaction between conduction electrons and 4f orbitals of Ce^{4+} ions in the CeO_2 matrix. These signals are also present on the EPR spectrum of the ceria support before impregnation. The A signal has been attributed to Ce^{3+} species with removable ligands and the B signal to Ce^{3+} ions stabilized by some lattice defects (CeO_{2-x}).[29] In fact, when heated at high temperature, ceria is known to show large deviations from its CeO_2 stoichiometric composition.[4,5,28] Moreover, in comparison with pure ceria,[18] we observed that the presence of vanadium ions in V−Ce−O samples stabilized the Ce^{3+} species, leading to an A signal, even at high temperature. It is important to notice that no signal relative to V^{IV} species has been observed, whatever the calcination temperature, demonstrating that the totality of the vanadium species are in the V^V oxidation state after the complete decomposition of vanadyl oxalate on the ceria carrier. This remark allows us to confirm the corresponding attribution of TG-DSC measurements given above.

From a calcination temperature of 600 °C, a new symmetric signal, denoted by S, centered at $g = 2.004$ with a line width of $\Delta H_{pp} = 11$ G, appears. The S signal is only observed while the EPR spectrum is recorded at −269 and −196 °C and not at 20 °C (Figure 5). To have a better resolution of the S signal, the recording of the EPR spectrum has been performed with a modulation amplitude higher (at −269 °C) than the one used for the two others spectra (−196 °C and 20 °C), which was fixed to 5 and 1 G respectively. Owing to these differences, broadness of the EPR lines (A and B signals, Mn^{2+} lines) can be observed at −269 °C. Nevertheless, the signal intensities were not affected, since the normalized double integration of the Bruker WIN EPR program[26] was used to compare intensities. In fact, we have observed that the evolution of A and B signals intensities verified the Curie law, as the increase of the intensities was related to the decrease of the recording temperature following ($I_1/I_2 = T_2/T_1$). Concerning the S signal, its increase in intensity with the decrease of recording temperature was much higher than the expected one. Such phenomenon can arise from paramagnetic species with short spin relaxation time. Moreover, at −196 °C, the S signal was broadened by spin−lattice interaction ($\Delta H_{pp} = 11$ G versus $\Delta H_{pp} = 5.8$ G at −269 °C). In fact, Watterich et al.[30] observed similar signals, with the same behavior versus recording tem-

(27) Aboukaïs, A.; Bennani, A.; Aissi, C. F.; Wrobel, G.; Guelton, M. *J. Chem. Soc., Faraday Trans.* **1992**, *88*, 1321.
(28) Fierro, J. L. G.; Soria, J.; Sanz, J.; Rojo, M. J. *J. Solid State Chem.* **1987**, *66*, 154.
(29) Martinez-Arias, A.; Fernandez-Garcia, M.; Belver, C.; Conesa, J. C.; Soria, J. *Catal. Lett.* **2000**, *65*, 197.

perature, attributed to trapped electron in oxygen vacancies (F centers) in TeO_2 crystals. This attribution appeared also in good agreement with the observations of Bobricheva et al.[31] in sulfated zirconia.

The appearance of the S signal can be related to the results already obtained above by Raman spectroscopy and TG-DSC, showing that for high-temperature treatment (>500°C), the amounts of V_2O_5 and CeO_2 phases decrease during the calcination of *x*V10Ce samples, whereas a new phase of $CeVO_4$ is revealed. In Figure 4, with the increase of calcination temperature from 600 to 700 °C, the intensity of the S signal strongly increases and then remains practically the same after the treatment at 800 °C. Simultaneously, a diminution in the intensity of the A and B signals is clearly obtained between 600 and 700 °C. It should be noticed that when a pure ceria support has been calcined at 700 °C, the absence of the S signal was revealed by EPR.[13] Thus, the single electron, responsible for the S signal, cannot be trapped in oxygen vacancies of the ceria matrix. All the *x*V10Ce samples, calcined at different temperatures, were also studied by EPR spectroscopy. The same behavior was observed concerning the evolution in intensity of the signal relative to electrons trapped in oxygen vacancies (signal S) and those corresponding to Ce^{3+} species (signals A and B). Thus, the EPR data tend to show that the appearance of the S signal can be correlated with the formation of the $CeVO_4$, while the diminution of signals relative to Ce^{3+} species in ceria can be explained by the CeO_2 consumption. In addition, the fact that the $CeVO_4$ phase formation is achieved at 700 °C could explain the stability in EPR signals intensities obtained between 700 and 800 °C.

Data on the chemical properties and thermal behavior of both ceria and vanadium oxide should be considered in order to put forward the evidence on how the single electron is trapped in the vanadium−cerium oxide matrix. It is well-known that the pure vanadium pentoxide[32] and the pure cerium oxide[19] lose oxygen at high calcination temperatures to give the nonstoichiometric oxides V_2O_{5-x} and CeO_{2-y}, respectively. Generally, the oxygen vacancies are formed and stabilized by vanadium or cerium ions in lower oxidation states (V^{4+} or Ce^{3+}). In the case of the *x*V10Ce solids, when the vanadium oxide supported on ceria is calcined at temperatures higher than 500 °C, the oxygen vacancies could be formed in CeO_2 and V_2O_5 phases. Simultaneously, redox reactions can be produced between the two couples Ce^{3+}/Ce^{4+} and V^{4+}/V^{5+} to give the $CeVO_4$ phase, formed of Ce^{3+} and V^{5+} species. The electrons exchanged between the redox couples can be trapped in the oxygen vacancies during their formation. Consequently, it can be assumed that under these experimental conditions, the single electron is trapped in the V−Ce oxide matrix in an oxygen vacancy in the $CeVO_4$ phase.

5. ^{51}V MAS NMR. Figure 6 illustrates ^{51}V MAS NMR spectra of *x*V10Ce samples calcined at 500 °C recorded

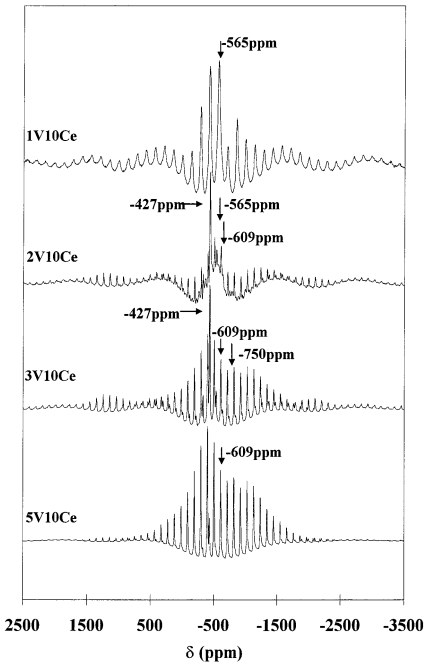

Figure 6. ^{51}V MAS NMR spectra of *x*V10Ce samples calcined at 500 °C. $\nu_R = 11$ kHz.

with a spinning frequency, $\nu_R = 11$ kHz. At low vanadium content (1V10Ce), the spectrum obtained reveals the presence of a species characterized by its isotropic component $\delta_{iso} = -565$ ppm and several associated spinning sidebands. This signal was also detected for 2V10Ce with low intensity. For the samples with higher vanadium content, a highly symmetric signal centered at $\delta_{iso} = -427$ ppm has been obtained. In addition, a signal at $\delta_{iso} = -750$ ppm with a weak intensity is evidenced only for the 3V10Ce sample. Finally, a signal centered at $\delta_{iso} = -609$ ppm and characterized by an asymmetry of the sidebands pattern appears in 2V10Ce and 3V10Ce samples and figures such as the predominant species in the 5V10Ce sample. This latter species is well-known and can be typically attributed to V_2O_5.[33−35]

Since the isotropic chemical shift cannot be used to elucidate the vanadium species coordination, the determination of NMR parameters was necessary to get accurate information concerning these species. Indeed, the spectroscopic parameter that differentiates between the various tetrahedral and octahedral vanadium(V) oxide coordination environments is the static NMR line shape, which is dominated by chemical shift anisotropy. Chemical shift anisotropy (CSA) parameters ($\Delta\delta$, $\eta\sigma$) and quadrupolar parameters (C_Q, η_Q) are obtained by simulation of the experimental spectrum using the QUASAR program elaborated by Amoureux and Fernandez.[36] The following conventions are used: chemical shift $\delta_{iso} = 1/3(\delta_1 + \delta_2 + \delta_3)$, with $|\delta_3 - \delta_{iso}| > |\delta_1 - \delta_{iso}| > |\delta_2 - \delta_{iso}|$. Table 3 gathered the values of NMR parameters

(30) Werich, A.; Kappers, L. A.; Gilliam, O. R.; Bartram, R. H.; Földvari, I.; Korecz, L. *Nucl. Instrum. Method Phys. Res. B* **2002**, *191*, 261.
(31) Bobricheva, I. V.; Stavitsky, I. A.; Yermolaev, V. K.; Kotsarenko, N. S.; Shmachkova, V. P.; Kochubey, D. I. *Catal. Lett.* **1998**, *56*, 23.
(32) Desagher, S.; Liang, T. Y.; Buvet, R. *J. Chim. Phys.* **1975**, *72*, 390.
(33) Lapina, B.; Mastikhin, V. M.; Shubin, A. A.; Krasilnokov, V. N.; Zamaraev, K. I. *Prog. NMR Spectrosc.* **1992**, *24*, 457.
(34) Skibsted, J.; Nielsen, N. C.; Bildsoe, H.; Jacobsen, H. J. *Chem. Phys. Lett.* **1992**, *188*, 405.
(35) Fernandez, C.; Bodart, P.; Amoureux, J.-P. *Solid State Nucl. Magn. Reson.* **1994**, *3*, 79.
(36) Amoureux, J. P.; Fernandez, C.; Carpentier L.; Cochon, E. *Phys. Status Solid A* **1992**, *132*, 461.

Table 3. NMR Parameter Values of Different Vanadium Species from Simulation of Experimental Spectra

δ_{iso} (ppm)	CSA (ppm)	$\eta\sigma$	C_Q (MHz)	η_Q	attribution
−565	786	0.10	1.42	0.90	distorted octahedral V−O−V chains
−750	352	0.05	4.14	0.20	distorted tetrahedral sites
−609	1030	0.24	0.83	0.06	V_2O_5[a]
−427	177	0.01	5.62	0.21	$CeVO_4$

[a] NMR parameter data from ref 35.

obtained for the signals with $\delta_{iso} = -427$, −565, −609, and −750 ppm.

The shape of the sideband pattern of species with $\delta_{iso} = -565$ ppm evidenced a distortion of the vanadium site. Moreover, the lines relative to this species appear rather broad, which could be correlated with an absence of regular ordering of these vanadium species. Using values of quadrupolar parameters ($C_Q = 1.42$ MHz and $\eta_Q = 0.9$) and chemical shift anisotropy parameters ($\Delta\delta = 786$ ppm, $\eta_\sigma = 0.1$), an almost axially symmetric chemical shift tensor was obtained. Considering the evolution of CSA parameters versus the vanadium coordination,[33] these values correspond with vanadium species in distorted octahedral environment. A comparison with CSA parameters values obtained for V_2O_5 also indicated a slightly lower distortion of the sites corresponding to $\delta_{iso} = -565$ ppm. Hence, in this low vanadium content solid (1V10Ce), these species are consistent with polymeric species V−O−V dispersed on the ceria surface.

The signal with $\delta_{iso} = -750$ ppm (Figures 6 and 7) exhibits a particularly high quadrupolar constant value $C_Q = 4.14$ MHz but a low chemical shift anisotropy $\Delta\delta = 352$ ppm. Similar features are obtained in the case of species at $\delta_{iso} = -427$ ppm: $C_Q = 5.62$ MHz and $\Delta\delta = 177$ ppm. In both cases, the large number of sidebands spread on each side of the isotropic component attested for high values of quadrupolar constant C_Q. It arises from important electric field gradient at the nucleus. Recently, it has been shown[37] that the signal with $\delta_{iso} = -427$ ppm corresponds to the tetragonal structure of cerium orthovanadate ($CeVO_4$), in which vanadium atoms are located at the center of isolated tetrahedra. The weak chemical shift anisotropy value clearly reflects the quite regular tetrahedral environment of vanadium in this structure. Since the CSA parameter is mainly related to the geometry of various vanadium polyhedra, the signal with $\delta_{iso} = -750$ ppm can be assigned to slightly distorted tetrahedral sites.[33]

In addition, the isotropic chemical shift δ_{iso} values relative to $CeVO_4$ ($\delta_{iso} = -427$ ppm) was evidenced to shift with the rotation frequency[37] in relation with the variations of sample temperature. Such phenomena were explained by an interaction between the unpaired $4f^1$ electrons of the Ce^{3+} ions of $CeVO_4$ with the nuclear spin of vanadium. In the present study, the same dependence of the δ_{iso} value of V−O−V species with $\delta_{iso} = -565$ ppm was also clearly revealed in 1V10Ce but not in the case of tetrahedral species ($\delta_{iso} = -750$ ppm) in 2V10Ce and 3V10Ce samples. For these reasons, it may be envisaged that V^{5+} ions as V−O−V chains ($\delta_{iso} = -565$ ppm) strongly interact with the surface of CeO_2 with substoichiometric character versus oxygen, which could imply the presence of Ce^{3+} species or trapped electrons in the solid. Such species were already evidenced above with the EPR technique. On the contrary, it is suggested that tetrahedral species exhibit lower interactions with the CeO_2 support. This interpretation will be supported by the rapid transformation of this species with the increase of calcination temperature (Figure 7). It also appears in good agreement with similar observations of Lapina et al.[33] in ^{51}V NMR studies of different vanadia-based oxide catalysts.

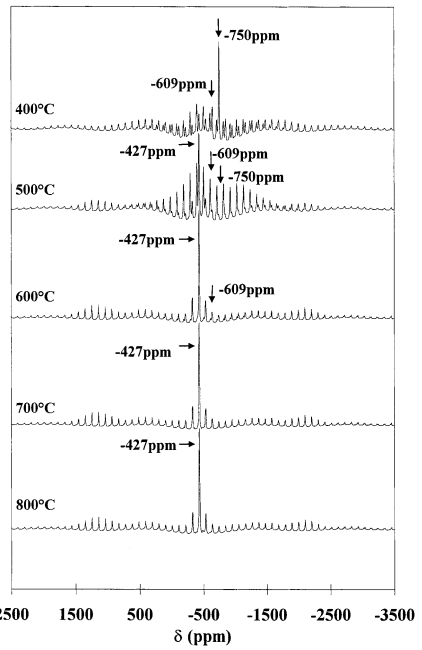

Figure 7. ^{51}V MAS NMR spectra of 3V10Ce sample calcined at different temperatures. $\nu_R = 11$ kHz.

To evaluate the stability and follow the evolution of the different vanadia species formed on the catalyst surfaces versus the thermal treatment of the samples, NMR spectra were recorded for each sample calcined at different temperatures between 400 and 800°C. An illustration is given in Figure 7 for the 3V10Ce sample. In fact, the spectrum of the latter sample, calcined at 400 °C, exhibits the signal relative to distorted tetrahedral sites ($\delta_{iso} = -750$ ppm) with large intensity in addition to the signal characteristic of polycristalline V_2O_5 ($\delta_{iso} = -609$ ppm). For the calcination temperatures higher than 400 °C, the intensity of the $\delta_{iso} = -750$ ppm signal drastically decreases. A progressive transformation of tetrahedral species was observed between 400 and 500 °C, which leads to the appearance of the cerium orthovanadate ($CeVO_4$) phase. However, one cannot exclude the partial agglomeration of tetrahedral species leading to the formation of the vanadium pentoxide phase. At higher temperature, it clearly appears that the formation of $CeVO_4$ is favored, whereas V_2O_5 is progressively and completely consumed, in agreement with the $V_2O_5 + 2CeO_2 \rightarrow 2CeVO_4 + {}^1/_2O_2$ reaction. The formation of the $CeVO_4$ phase at high temperature is observed for all the samples. No other V−Ce−O phase was evidenced in our study. From the thermodynamic approach proposed by Yokokawa et al.,[38] only mixed

(37) Cousin, R.; Courcot, D.; Abi-Aad, E.; Capelle, S.; Amoureux, J. P.; Dourdin, M.; Guelton, M.; Aboukaïs, A. *Colloids Surf. A* **1999**, *158*, 43.

(38) Yokokawa, H.; Sakai, N.; Kawada, T.; Dokiya, M. *J. Am. Ceram. Soc.* **1990**, *73*, 649.

phases like $CeVO_4$ and $CeVO_3$, where atomic ratio V/Ce = 1, can be formed at high temperature in V−Ce−O systems, whatever the vanadium content. This particularity can be partially explained by the large stabilization energy of $CeVO_4$. Moreover, low oxygen partial pressure or reducing atmosphere conditions are necessary to stabilize the $CeVO_3$ phase.[39] On the other hand, in the case of others rare earth−vanadium oxide systems, it is known that several mixed phases can be formed mainly following the vanadium content, for instance, compounds such as La_3VO_7 and $LaVO_4$ in the case of La−V−O systems.[38]

In the present work, the vanadium species stabilized at low temperatures (≤550 °C) are depending on the vanadium content. In this way, polymeric V−O−V species were found to be stabilized in 1V10Ce and 2V10Ce samples until 550 °C. However, this species represent the totality of the vanadium compound on 1V10Ce (Figure 6), whereas for 2V10Ce it represents a minor species. Increasing the vanadium content from 2V10Ce to 3V10Ce leads to an increased amount of the tetrahedral species, mainly stable till 450 °C. In the case of a high amount of vanadium (5V10Ce), only the V_2O_5 phase was formed from 400 °C.

Important differences appear in the nature of the supported VO_x species present under ambient conditions and following the vanadium content. These differences can be discussed from the chemistry of vanadium(V) mentioned in the literature.[40−42] According to Deo et al.,[40] different vanadate species can be stabilized on the oxide surfaces. The stabilization depends on the vanadium concentration and the acido-basic properties of the solid surfaces. Indeed, it is known[42] that the formation of V−O−V polymers can be obtained at high vanadium concentration but under acidic conditions. On the contrary, under basic conditions, the formation of pyro-, mono-, and orthovanadate can be formed at low vanadium concentration. In addition, Deo et al.[40] related the structure of VO_x entities formed on the solid surface to the pH value at zero point charge of the surface. In the case of CeO_2 surface, the pH value is equal to 6.8, and this value can explain the stabilization of $(VO_3)_n$ metavanadates on the ceria surface with a tetrahedral environment.[43] Since in our case the V−Ce systems were prepared from $VOC_2O_4/H_2C_2O_4$ solution and CeO_2 solid, the net catalyst surface pH at zero point charge (pH zpc) can control the molecular structure of vanadia impregnated on oxide carriers. In the case of ceria, it could mainly account for the stabilization of tetrahedral species in 2V10Ce and 3V10Ce, whereas in 5V10Ce, a higher vanadium amount and a more acidic medium may explain the V_2O_5 formation. On the contrary, these consideration could not explain the formation of bidimensionnal V−O−V chains, which were clearly stable on ceria till 550 °C. In fact, we demonstrated that this species interact with Ce^{3+} ions or trapped single electrons near the CeO_2 surface. Particularly in this case, the formation of the vanadium species is rather dependent on the ability of cerium oxide carrier to give rise to electron transfers toward the vanadium atoms of the vanadia phase.

The formation of $CeVO_4$ upon increasing the temperature is found to depend on the vanadium content and hence the vanadium species stabilized after a calcination treatment at lower temperature. Indeed, polymeric vanadium species (1V10Ce) exhibit a relatively good stability in comparison with other species present at 500 °C. This fact was also clearly revealed in the TG-DSC study, where the mass loss corresponding to $CeVO_4$ formation occurred at a temperature close to 600 °C, whereas it starts at 500 °C on other samples. Then, it is suggested that tetrahedral species and V_2O_5 phase behave as precursors that favor the formation of $CeVO_4$ phase. Besides, it has to be mentioned that the high specific area of CeO_2 carrier (100 m^2/g) and hence the presence of CeO_2 nanoparticles is a favorable parameter for the dispersion of vanadium ions on ceria surface. These properties probably have to be taken into account toward the formation of the different vanadium(V) species and also toward the formation of the $CeVO_4$ phase at relatively low temperature.

Conclusion

The combination of different physicochemical techniques used in this study has allowed us to define the nature and evaluate the stability of different vanadium oxide species present in the V−Ce−O compounds calcined at different temperatures from 400 to 800°C. In the temperature range of 400−550 °C, polymeric V−O−V chains, in interaction with Ce^{3+} ions or trapped electrons, are identified on the ceria surface for low vanadium content (1V10Ce). Vanadium tetrahedral surface species and polycrystalline V_2O_5 phase were evidenced at higher vanadium loading. These latter phases tend to react with ceria from 500 °C to lead to the formation of the $CeVO_4$ phase, whereas it occurred near 600 °C in the case of V−O−V species, owing to their higher stability. During the reaction, a single electron is trapped in an oxygen vacancy in the $CeVO_4$ phase and can be considered as a probe to the $CeVO_4$ phase presence.

Acknowledgment. The authors would like to thank the "Conseil Général du Nord", the "Région Nord-Pas de Calais", and the European Community (European Regional Development Fund) for financial supports in the EPR and the Thermal Analysis apparatus purchase. Also, the authors thank B. Revel for assistance with the NMR measurements.

CM010396T

(39) Matta, J.; Abi-Aad, E.; Courcot, D.; Aboukaïs, A. *NATO ARW, IX International Symposium on Magnetic Resonance in Colloid and Interface Science*; St Petersburg, Russia, June 26−30, 2001.
(40) Deo, G.; Wachs, I. *J. Phys. Chem.* **1991**, *95*, 5889.
(41) Taouk, B.; Guelton, M.; Grimblot, J.; Bonnelle, J. P. *J. Phys. Chem.* **1988**, *92*, 6700.
(42) Baës, C. F.; Mesmer, J. *The hydrolysis of cations*; Wiley: New York, 1970.
(43) Brunelle, J. P. *Pure Appl. Chem.* **1978**, *50*, 1211.